JOURNAL OF Materials CHEMISTRY

Phosphate liquid crystals: novel supramolecular template for the synthesis of lamellar aluminophosphates with natural form

Scott R. J. Oliver and Geoffrey A. Ozin*

Materials Chemistry Research Group, Lash Miller Chemical Laboratories, University of Toronto, 80 St. George Street, Toronto, Ontario, Canada M5S 3H6

The thermal properties of *n*-alkylammonium dihydrogenphosphates, $[C_nH_{2n+1}NH_3^+][H_2PO_4^-]$, where $6 \leqslant n \leqslant 18$, have been investigated for the first time. It was discovered that for decylammonium ($n=10$), the material undergoes several polymorphic phase transitions before ultimately transforming to a smectic liquid crystal mesophase. The crystal to liquid crystal transformation of this phase was studied by *in situ* variable temperature polarizing optical microscopy and revealed intriguing micron dimension surface patterns. Similar thermal behaviour was observed when the material was dispersed in a polyethylene glycol non-aqueous solvent. The results have direct implications for the growth and form of surface patterned lamellar aluminophosphate morphologies prepared organo-thermally from aluminium oxide, phosphoric acid and *n*-alkylamines in polyethylene glycol-based solvents. Topological defects present in the precursor alkylammonium phosphate mesophase appear to be responsible for the emergence of surface textured lamellar aluminophosphate replica materials with biomimetic form. Phosphate liquid crystals represent a new class of supramolecular templates for the synthesis of a wide variety of mesostructured metal phosphates.

Introduction

Mineralization of supramolecular organic templates leads to inorganic materials with complex form.[1] The length scale of structural features spans angstroms to millimetres, the architectures are hierarchical, and the morphologies and surface patterns display natural form.[2,3] Templates that have been used for this kind of morphosynthesis include surfactant-based micelles, hexagonal and lamellar liquid crystal mesophases, vesicles and oil–water microemulsions.[1–14] Condensation polymerization reactions in the phase-separated boundary regions delineated by polar headgroups lead to the deposition of inorganics and the production of mesoporous and mesolamellar inorganic materials[15] with spatial control of morphology over all three spatial dimensions.[1–14]

In the course of our work on the organothermal synthesis of aluminophosphates using oligoethylene glycol solvents, we discovered mesolamellar aluminophosphates (MLAs) with biomimetic form.[2,4–7,12] They are composite inorganic–organic materials where anionic aluminophosphate layers are separated by bilayers of charge-balancing $[C_nH_{2n+1}NH_3^+]$ alkylammonium cations, as evidenced by powder X-ray diffraction (PXRD), transmission electron microscopy (TEM), solid state nuclear magnetic resonance (NMR) and a variety of other techniques.[12,16] The alkylamine chain lengths that lead to this type of layered material are $6 \leqslant n \leqslant 18$. However, for the range $8 \leqslant n \leqslant 11$, materials emerge with spectacular morphologies and filigree surface patterns that resemble those found in single cell marine organisms with mineral shells, such as the radiolaria.[2,4–7] MLA morphologies appear as millimetre dimension solid and hollow spheres with ornate surface patterns on the micron scale. After our initial reports, others recognized the same MLA materials for $n=6$,[17,18] $n=8$,[18] $n=10$[18] and $n=12$,[18,19] and extended the morphosynthesis paradigm[2] to include mesolamellar aluminium oxides which produced similar types of surface designs.[20] Despite all of this effort to create shapes synthetically, the details of the morphogenesis process remained obscure.

During this and other related work, we also discovered that the starting reaction mixtures contain a highly crystalline alkylammonium phosphate salt.[16,21,22] This was the case for all of the $C_nH_{2n+1}NH_2$ alkylamines, for $n=1$–18, as well as for a variety of other primary and secondary amines. We have recently completed the crystal structures for octylammonium ($n=8$) and decylammonium ($n=10$) containing dihydrogenphosphate ($H_2PO_4^-$) as the charge-balancing anion.[22] The phosphates are arranged in layers and are separated by interdigitated alkylammoniums.

Here, we report the characterization of the decylammonium dihydrogenphosphate (DDP) solid phase. Using a variety of techniques, the data show that the material undergoes a series of thermal transitions, where the alkylammonium molecules first de-interdigitate in a crystal-to-crystal transition, followed by the formation of a thermotropic smectic phosphate liquid crystal phase. A series of remarkable patterns emerge for the material under these conditions, particularly if it is dispersed in a polyethylene glycol non-aqueous solvent. We propose that these patterns arise from topological defects in the DDP liquid crystal and, when generated under synthesis conditions in the presence of an Al^{III} precursor, are responsible for the growth of surface patterned lamellar aluminophosphate morphologies with natural form.

Experimental

Synthesis

All of the alkylammonium phosphate salts can be prepared as a suspension of small, colourless crystals in any of a number of solvents such as water, methanol and tetraethylene glycol (TEG). This was achieved simply by adding phosphoric acid (85 mass%, Aldrich) to the solvent, followed by an alkylamine (Aldrich) in equimolar amounts. The slurry had the same phase and consistency whether or not a source of aluminium oxide was added. In some cases, the slurry was examined. For analysis specifically of the phosphate salt, a dry powder of the material was obtained by filtering the slurry and washing with acetone.

Powder X-ray diffraction (PXRD)

Powder patterns were collected on a Siemens D5000 diffractometer (Cu-Kα radiation, $\lambda = 1.54178$ Å). The step size was 0.030°, step time 1.0 s and scan range 1 to 50° (2θ). The detector in the instrument was a Kevex 2005–212 solid state detector. *In situ* variable-temperature (VT) PXRD patterns were obtained on the same instrument under a nitrogen flow,

using a Siemens HTK 10 attachment. The heating rate was 1 °C min^{-1} between scans, and the temperature was held constant during data collection. Quick scans were run from 1 to 37° (2θ), with 0.050° step size and 0.7 s step time.

Differential scanning calorimetry (DSC)

Differential scanning calorimetry was performed on a Perkin Elmer 7 Series Analyzer, with a heating rate of 5 °C min^{-1} and continuous temperature cycling between 25 °C and 100 °C. Approximately 10 mg of ground sample was accurately weighed and sealed in an aluminium sample holder.

Variable temperature polarizing optical microscopy (POM)

Variable temperature optical microscopy was performed on an Olympus BH-2 equipped with a variable temperature hot-stage attachment. A camera was used to capture images in converging white light that was either plane-polarized or with analyzer and polarizer crossed. The temperature could be controlled and stopped when necessary. Temperatures ranged between 25 °C and 120 °C and the rate of change of temperature was 5 °C min^{-1}.

Results and Discussion

Characterization of DDP, [$C_{10}H_{21}NH_3^+$][$H_2PO_4^-$]

The single crystal structure of DDP has been previously published.[4,22] Its interlayer distance is approximately 19.8 Å. The ^{31}P MAS NMR spectrum showed two sharp resonances of equal intensity at 1.13 and −0.65 ppm (spinning rate 6 kHz, referenced to $NH_4H_2PO_4$), one for each of the two crystallographically unique dihydrogenphosphate anions in the asymmetric unit. The ^{13}C CP MAS NMR spectrum displayed peaks in the regions expected for decylammonium,[23] from 13.66 ppm for the methyl end of the alkyl chain to 40.46 ppm for the α-carbon, with a general increase in fwhm of the peaks.[16]

The thermal properties of DDP were investigated and showed several surprising transitions. An initial *in situ* VT-PXRD study of DDP revealed that several transitions occur between 25 °C and 125 °C, Fig. 1(a). The new phase that is present at 125 °C remains intact until it collapses at approximately 350 °C. Accordingly, the TGA of DDP remains unaltered with little or no mass loss up to 300 °C and then undergoes rapid mass loss (not shown).

Closer investigation by VT-PXRD between 25 °C and 125 °C showed that a crystal-to-crystal transition occurs between 80 °C and 90 °C, Fig. 1(b). Note the series of distinct peaks for each phase and that the process is completely reversible: the second crystalline phase reverts back to the original DDP structure between 80 °C and 50 °C. The lowest-angle, majority peak shifts to lower angle and a greater *d*-spacing of *ca.* 24.0 Å for the higher-temperature phase.

It was also observed that at slightly higher temperature, the second phase in turn converts to a third phase between 100 °C and 110 °C, Fig. 1(c). The layer to layer *d*-spacing of this third phase is approximately 25.7 Å. The only other peaks are the second and third order reflections, Fig. 1(a) and (c). The third phase reverts to the second and first crystalline phases at approximately 90 °C and 70 °C, respectively, Fig. 1(c). All transitions were reversible and may in fact be continuously cycled, with increase in diffraction intensity (and extent of order) of the DDP phase after each cycle. Accounting for the peaks of these three phases, it appears that another phase is present in the patterns of 90 °C and 80 °C, Fig. 1(c).

These transformations may be followed in the DSC of DDP, Fig. 2. The precise recurrence and reversibility of the process can be seen in the three cycles shown, as well as a hysteresis of 5 to 15 °C for each step. All transitions are endothermic on the heating cycle (top) and appear as exothermic events on cooling (bottom). The first transition (*ca.* 82 °C upon heating and *ca.* 65 °C upon cooling) involves a large enthalpy change in both directions. The second transition corresponds to the broad peak which begins before 90 °C, centred at *ca.* 93 °C and the third to the sharp peak at *ca.* 95 °C. These two peaks are overlapped during increase of temperature, but occur at different temperatures during cooling (*ca.* 82 °C and 92 °C,

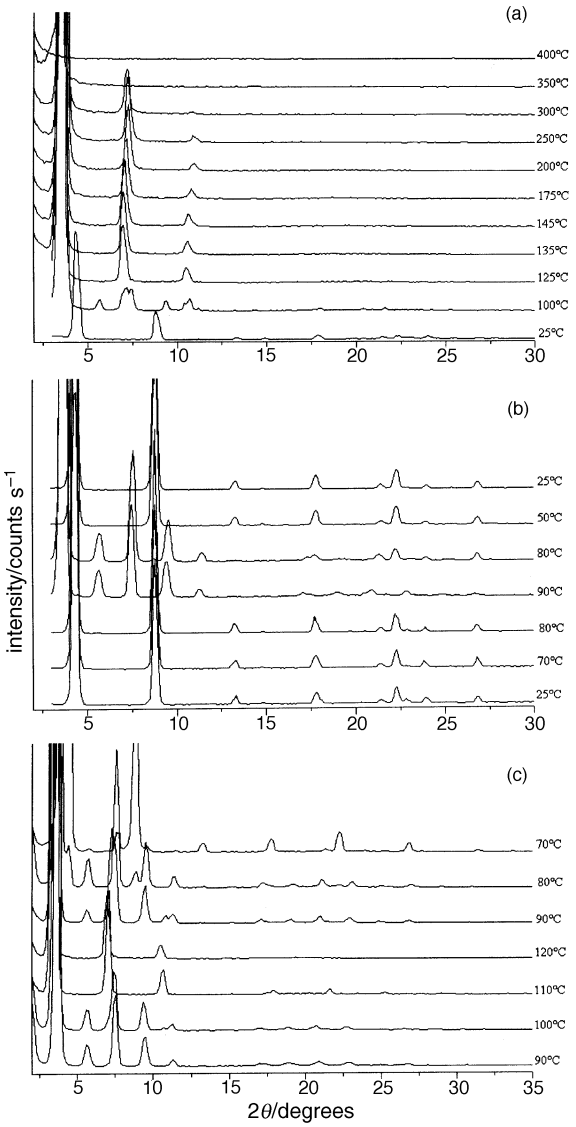

Fig. 1 VT-PXRD of DDP. (a) Initial VT-PXRD collected from 25 °C to 400 °C. (b) Closer investigation of the first transition between 80 °C and 90 °C. (c) The second transition occurs between 100 °C and 110 °C.

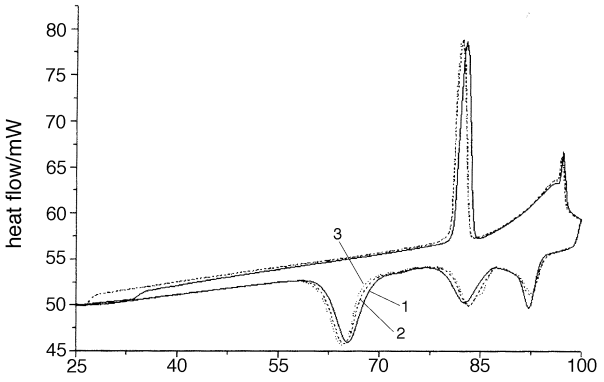

Fig. 2 DSC trace of DDP. The three cycles display the reproducibility and reversibility of the thermal transitions.

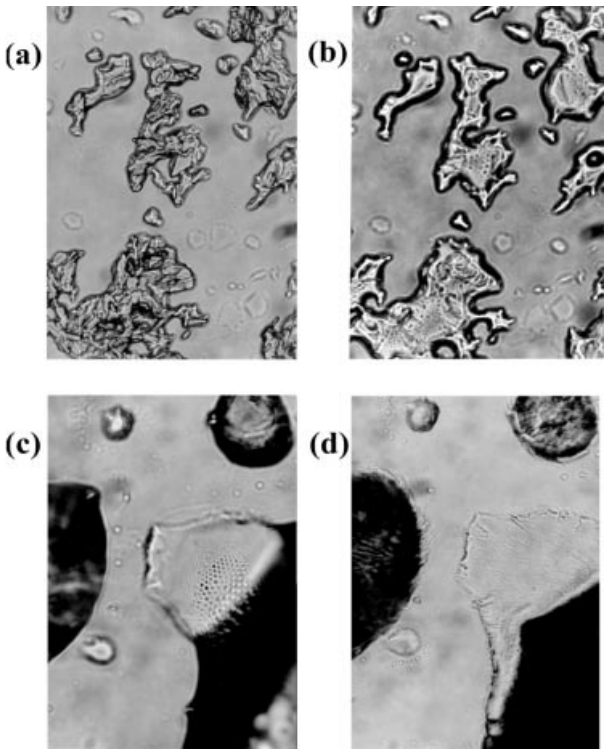

Fig. 3 Optical micrographs of DDP (magnification $\times 500$). (a) The DDP powder at 95 °C, comprised of small needles. (b) The same area shown at 100 °C, where the crystals have fused together to form larger particles with an interesting morphology. (c) Another area also at 100 °C, showing more developed bowl-like impressions and a size gradient across the surface. (d) The same area as in (c) after cooling to 70 °C, where the material has recrystallized to DDP.

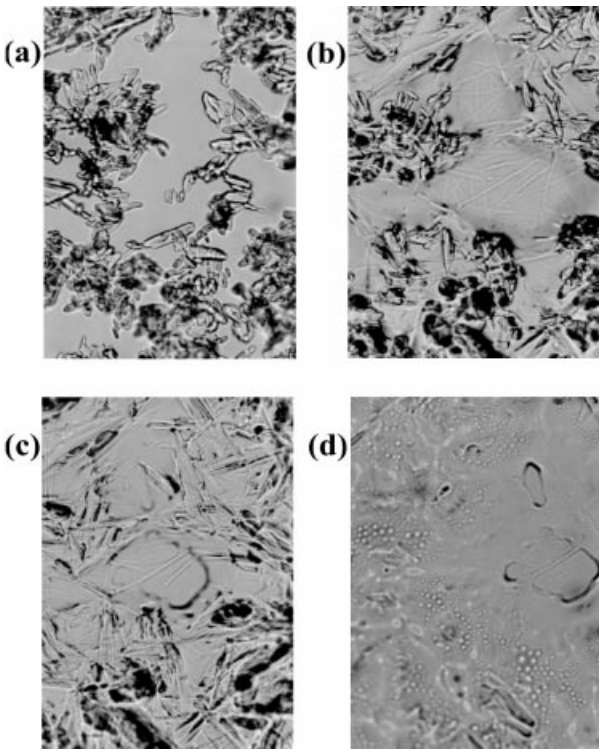

Fig. 4 Optical micrographs of DDP dispersed in a TEG solvent (magnification $\times 500$). All images are shown for the same area of sample. (a) The DDP crystals at 70 °C, showing the same morphology as for the powder itself. (b) At 85 °C, the crystals begin to fuse and long needles are formed. (c) The process continues at 90 °C. (d) At 98 °C, the needles have disappeared and a continuous morphology of surface bowls is formed.

respectively). This would account for the appearance of other peaks at 90 °C and 80 °C during only the cooling cycle of the VT-PXRD, Fig. 1(c).

In light of the above results, a variable temperature POM study was carried out for the DDP solid. The starting powder is comprised of small needles, Fig. 3(a). The temperature was slowly increased and at 100 °C, the crystals were observed to fuse together and circular bowl-like impressions could be observed on the particle surface, Fig. 3(b). The diameter of these features is of the order of 1–10 μm and their ordering is in some cases quite extraordinary, Fig. 3(c). The reversibility of the transitions is shown by the loss of these surface patterns when DDP recrystallizes upon cooling, Fig. 3(d). Again, these two states reversibly form by cycling the temperature of the hot-stage.

Micrographs were also collected for DDP dispersed in a TEG solvent, Fig. 4. The small crystals that were present initially, Fig. 4(a), begin to fuse together, while at the same time long thin needles form, Fig. 4(b) and (c). Both of these give way at 98 °C to a dominant morphology of circular impressions, which is present over the entire sample, Fig. 4(d). In Fig. 5 this morphology is seen along with a corresponding image of the sample between crossed polars. The latter, Fig. 5(b) and (d), show optical birefringence, which is diagnostic of the texture of a thermotropic smectic liquid crystal.[24] Extinction is observed in the directions corresponding to the axes of the crossed polars. Note the close-packing of the surface impressions and that the size range is approximately 1 to 50 μm.

When the DDP solid is simply heated on a hot plate above its liquid crystal transition temperature, it becomes a soft, semi-translucent paste. It was also observed that heating the mesolamellar aluminophosphate (MLA) synthesis mixture (*i.e.*, an opaque, white, viscous TEG–pseudoboehmite–DDP slurry) in a beaker to *ca.* 55 °C, the mixture separated into an orange

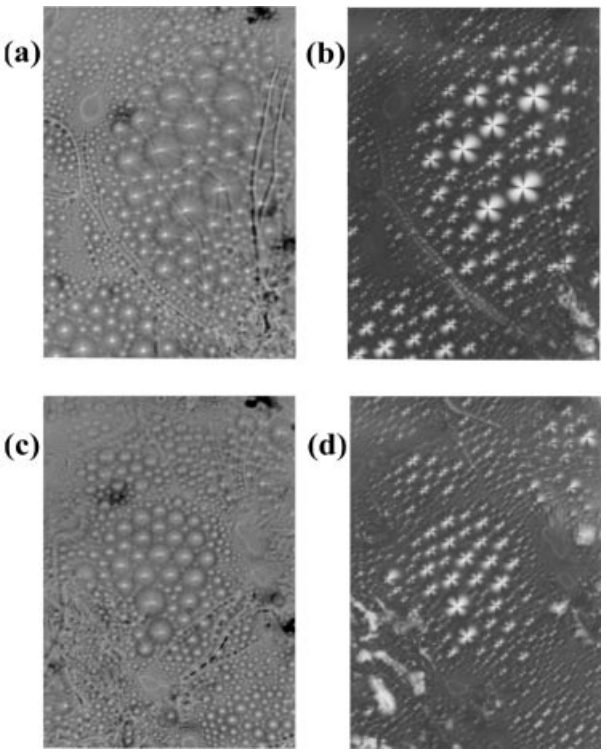

Fig. 5 Optical micrographs of DDP dispersed in TEG (magnification $\times 500$). (a) This morphology is present throughout the sample at 99 °C. (b) The same area as in (a), between crossed polars. (c) Another area of the sample at 120 °C. (d) The same area as in (c), between crossed polars.

coloured liquid with a clump of soft material suspended in the solvent. In both cases, the soft material hardens upon cooling to room temperature.

This solid is therefore attributed to the DDP liquid crystal phase that has been directly observed in Fig. 4 and 5. It should be noted that since the DDP thermal transitions are completely reversible, the temperature dependent studies had to be performed *in situ* to observe these effects. These transitions must have occurred in other analogous syntheses which gave only DDP products, namely under hydrothermal conditions, in a TEG–silica–DDP experiment or in the absence of pseudoboehmite.[16,22]

Decylamine–MLA

The characterization of the MLA materials, synthesized using decylamine and undecylamine, was achieved in a multi-analytical SEM, TEM, PXRD, VT-PXRD, TGA, DSC and MS investigation.[2,4–7,12,16] Chemical analysis of the as-synthesized decylamine-related MLA (decylamine–MLA) showed it to contain 41.70 mass% C, 4.62 mass% N, 4.55 mass% Al and 10.49 mass% P, giving an overall molar ratio of $Al_{1.00}P_{2.02}C_{20.61}N_{1.96}$.

TEM images of microtomed sections of the MLA materials of varying $C_nH_{2n+1}NH_3^+$ alkylammonium chain length, $6 \leqslant n \leqslant 18$, displayed a well organized multilayer structure with an interlayer separation in agreement to that observed by PXRD.[12] The observation of only strong, low angle reflections in the PXRD patterns implies that the roughly 5 Å thick aluminophosphate lamellae are amorphous but are able to define a mesostructure having long range periodicity. The PXRD patterns also confirm that the interlayer *d*-spacing scales with the number of carbons in the alkane chain, Fig. 6(a), where its slope (*ca.* 2.05 Å per carbon) implies a fully extended bilayer conformation.

The ^{31}P MAS NMR spectrum of decylamine–MLA (spinning rate 10 kHz, referenced to 85 mass% H_3PO_4) displayed at least four distinct peaks in the −20 to 0 ppm range, assignable to four-coordinate phosphate groups. These are attributed to doubly and triply bridging phosphate groups in different chemical environments, which are the only types of phosphates that exist in any of the crystallographically defined layered aluminophosphates known to date.[25] The ^{27}Al MAS NMR spectrum of decylamine–MLA [spinning rate 13.0 kHz, referenced to $Al(H_2O)_6^{3+}$] shows two peaks at 48.7 and 0.0 ppm, corresponding to tetrahedral and octahedral aluminium, respectively. A third peak of much smaller intensity and integrated area was also observed between these two, at 23.9 ppm, and is best attributed to unreacted pseudoboehmite or pentacoordinate aluminium. These values of chemical shifts are similar to those typically observed in open-framework aluminophosphates.[26–29] The ^{13}C MAS NMR spectrum of decylamine–MLA was similar to that of DDP, but all of the peaks in this case were broader, particularly for the α and neighbouring carbons.

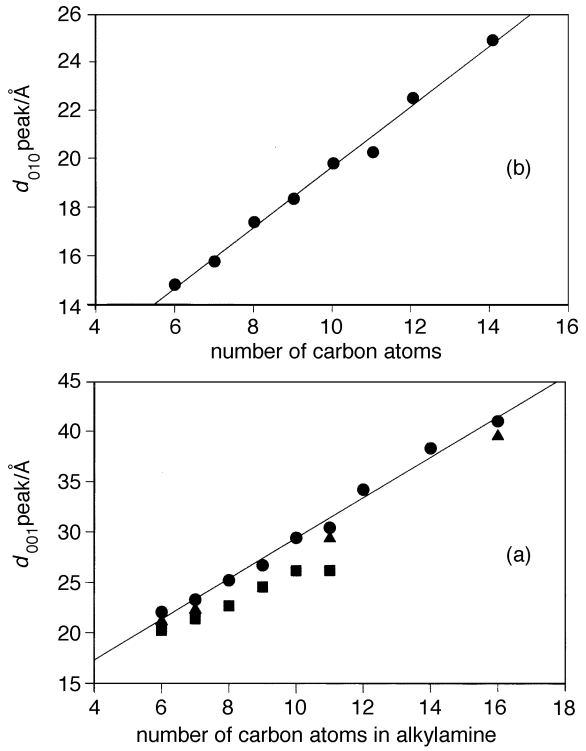

Fig. 6 Plots of interlayer spacing *versus* alkylamine carbon chain length. (a) The series of synthesized MLA materials. The triangles and squares represent the second and/or third MLA *d*-spacing observed in the PXRD of the product. (b) The series of synthesized alkylammonium phosphates.

DDP: liquid crystal formation and a supramolecular template for surface patterned MLA morphologies

As discovered in the single crystal structure analyses, the alkylammonium phosphate salts for $n=8$ and $n=10$ have their alkyl chains interdigitated.[4,22] The interlayer *d*-spacing for the series of phosphate salts also increases with alkyl chain length, Fig. 6(b), but at an expectedly slower rate (*ca.* 1.25 Å per carbon) than for the bilayer MLA material. An interdigitated arrangement is favourable when a relatively larger space needs to be filled by the alkyl chain,[30] and in order to maintain electroneutrality with the anionic layers.

The first strongly endothermic thermal transition of DDP involved the formation of a second crystalline phase of a larger interlayer spacing. This is attributed to the de-interdigitation of the DDP phase. Note that this transition is not gradual but rapid, as indicated by the sudden change of VT-PXRD patterns and the narrowness of the DSC peak, which is indicative of a first order phase transition. The transition to a second crystalline phase was observed followed by a more gradual, second order type transition to a thermotropic lamellar liquid crystal phase. Such interdigitated to liquid crystal bilayer transitions (and the reverse) commonly occur for phospholipid membranes and vesicles.[31–34] Often, these observations are also made by DSC and VT-PXRD.

The unique structural aspects of DDP are probably the reasons for its thermal behaviour. To begin, it is the only alkylammonium phosphate crystal structure known to date to contain an alkyl chain that is sufficiently amphiphilic to form a liquid crystal phase. This cannot occur for the phosphate salts of other amines, such as ethylenediamine.[35] Secondly, other known phosphate salts, such as cyclopentylammonium monohydrogenphosphate[22] and ethylenediammonium monohydrogenphosphate,[35] contain disjointed phosphate layers that are hydrogen-bonded into dimers or chains. In DDP, however, a continuous hydrogen-bonded sheet exists, where each phosphate donates and accepts two strong hydrogen bonds to define a layer of 'four-rings'.[22]

Liquid crystals, encompassing a wide variety of organic anisotropic structural units, can display surface patterns of the type described above. They originate from topological defects known as focal conics.[24,36,37] To expand further, the observed morphology–surface pattern–mesostructure relations for the DDP reactant and the mineralized MLA products allow one to formulate a rudimentary model for the morphogenesis of shapes and patterns in the TEG–pseudoboehmite–phosphoric acid–decylamine synthesis system.[4] In essence, the DDP exists as a smectic phosphate liquid crystal in the temperature range 150–180 °C used for the MLA synthesis. Reaction with the Al^{III} precursor leads to condensation–polymerization reac-

tions, $AlOH + POH \rightarrow Al-O-P + H_2O$, at the surface of a phosphate liquid crystal and the development of aluminophosphate contour surfaces that replicate the macro- and meso-structure of the liquid crystal. It is possible that, because of the presence and generation of small amounts of water in this non-aqueous synthesis system, the growth and form of surface patterned MLA shapes originate instead from a liquid crystal DDP–H_2O–TEG microemulsion templating pathway.[38] To date, this is our best model to account for the remarkable biomimetic form of surface decorated solid and hollow spheroidal MLA morphologies.[2,4–7,12,16]

Conclusions

An alkylammonium dihydrogenphosphate salt has been observed to de-interdigitate and form a thermotropic smectic liquid crystal mesophase. The phosphate liquid crystal phase, either pure or dispersed in the non-aqueous solvent tetraethyleneglycol, displays a series of impressive micron dimension surface patterns that appear to be imprinted in lamellar aluminophosphate morphologies prepared under the same experimental conditions but in the presence of an Al^{III} precursor. With this new found knowledge, it may be possible to control the topological defects in a variety of phosphate liquid crystals aimed at the synthesis of, for example, meso- and macro-structured aluminium, vanadium, iron, zinc, molybdenum, tin, zirconium or calcium phosphates, where the form and texture of the materials determines their function and utility in catalysis, agricultural, light emission and biomedical applications.

Financial support from the Natural Sciences and Engineering Research Council (NSERC) is deeply appreciated. S. O. is appreciative of an Ontario Graduate Scholarship and a University of Toronto Fellowship held during this work.

References

1 S. Mann and G. A. Ozin, *Nature* (*London*), 1996, **382**, 313.
2 G. A. Ozin, *Acc. Chem. Res*., 1997, **30**, 17.
3 S. Mann and D. Walsh, *Chem. Br*., 1996, **32**, 31.
4 S. Oliver, A. Kuperman, N. Coombs, A. Lough and G. A. Ozin, *Nature* (*London*), 1995, **378**, 47.
5 S. Oliver, N. Coombs and G. A. Ozin, *Adv. Mater*., 1995, **7**, 931.
6 S. Oliver and G. A. Ozin, *Adv. Mater*., 1995, **7**, 943.
7 S. Oliver, N. Coombs, D. Khushalani, A. Kuperman and G. A. Ozin, in *NATO Adv. Res. Workshop Proc.: Modular Chemistry*, Aspen, Colorado, 1995, ed. J. Michl, Kluwer, Dordrecht, 1997.
8 H.-P. Lin and C.-Y. Mou, *Science*, 1996, **273**, 765.
9 G. A. Ozin, D. Khushalani and H. Yang, in *NATO Adv. Res. Workshop Proc.: Supramolecular Chemistry*, ed. J. Wuest, Val Morin, Quebec, 1996.
10 S. Schacht, Q. Huo, I. G. Voigt-Martin, G. D. Stucky and F. Schüth, *Science*, 1996, **273**, 768.
11 P. T. Tanev and T. J. Pinnavia, *Science*, 1996, **271**, 1267.
12 N. Coombs, D. Khushalani, S. Oliver, G. A. Ozin, G. C. Shen, I. Sokolov and H. Yang, *J. Chem. Soc., Dalton Trans*., 1997, 3941.
13 G. A. Ozin, H. Yang and N. Coombs, *Nature* (*London*), 1997, **386**, 692.
14 G. A. Ozin, H. Yang and N. Coombs, *Adv. Mater*., 1997, **9**, 662.
15 C. T. Kresge, M. Leonowicz, W. J. Roth, J. C. Vartuli and J. C. Beck, *Nature* (*London*), 1992, **359**, 710.
16 S. Oliver, PhD Thesis, University of Toronto, 1997.
17 Q. Gao, R. Xu, J. Chen, R. Li, S. Li, S. Qiu and Y. Yue, *J. Chem. Soc., Dalton Trans*., 1997, 3303.
18 (*a*) A. Sayari, V. R. Karra, J. S. Reddy and I. L. Moudrakovski, *Chem. Commun*., 1996, 411; (*b*) A. Chenite, Y. Le Page, V. R. Karra and A. Sayari, *Chem. Commun*., 1996, 413.
19 Q. Gao, J. Chen, R. Xu and Y. Yue, *Chem. Mater*., 1997, **9**, 457.
20 M. Yada, H. Kitamura, M. Machida and T. Kijima, *Langmuir*, 1997, **13**, 5252.
21 S. R. J. Oliver, A. J. Lough and G. A. Ozin, *Z. Kristallogr., New Crystal Structures*, in press.
22 S. R. J. Oliver, A. J. Lough and G. A. Ozin, *Inorg. Chem*., submitted.
23 *The Aldrich Library of* ^{13}C *and* ^{1}H *FT NMR Spectra*, ed. C. J. Pouchert and J. Behnke, Aldrich Chemical Co., Milwaukee, 1993.
24 D. Demus and L. Richter, *Textures of Liquid Crystals*, Verlag Chemie, New York, 1982.
25 S. Oliver, A. Kuperman and G. A. Ozin, *Angew. Chem., Int. Ed. Engl*., 1998, **37**, 46.
26 C. S. Blackwell and R. L. Patton, *J. Phys. Chem*.,1984, **88**, 6135.
27 C. S. Blackwell and R. L. Patton, *J. Phys. Chem*., 1988, **92**, 3965.
28 H. He and J. Klinowski, *J. Phys. Chem*., 1993, **97**, 10385.
29 M. P. J. Peeters, L. J. M. van de Ven, J. W. de Haan and J. H. C. van Hooff, *J. Phys. Chem*., 1993, **97**, 8254.
30 See, for example, C. J. Bowlas, D. W. Bruce and K. R. Seddon, *Chem. Commun*., 1996, 1625.
31 V. Skita, D. W., Chester, C. J. Oliver, J. G. Turcotte and R. H. Notter, *J. Lipid Res*., 1995, **36**, 1116.
32 S. Maruyama, H. Matsuki, H. Ichimori and S. Kaneshina, *Chem. Phys. Lipids*, 1996, **82**, 125.
33 I. Hatta, S. Kato and H. Takahashi, *Phase Transitions*, 1993, **45**, 157.
34 F. S. Hing and G. G. Shipley, *Biochemistry*, 1995, **34**, 11 904.
35 (*a*) M. T. Averbuch-Pouchot and A. Durif, *Acta Crystallogr., Sect. C*, 1987, **43**, 1894; (*b*) S. M. Golubev and Y. D. Kondrashev, *Zh. Strukt. Khim*., 1984, **25**, 471; (*c*) S. Kamoun, A. Jouini, M. Kamoun and A. Daoud, *Acta Crystallogr., Sect. C*, 1989, **45**, 481; (*d*) M. Bagieu-Beucher, A. Durif and J. C. Guitel, *Acta Crystallogr., Sect. C*, 1989, **45**, 421.
36 M. Steers, M. Kleman and C. Williams, *J. Phys. Lett*., 1974, **35**, L21.
37 R. Deschenaux, E. Serrano and A. Levelut, *Chem. Commun*., 1997, 1577.
38 *The Colloidal Domain where Physics, Chemistry, Biology and Technology Meet*, ed. D. F. Evans and H. Wennerström, VCH, New York, 1994.

Paper 7/08598B; *Received* 28*th November*, 1997